Lost in Transition: Start-Up of Glycolysis Yields Subpopulations of Nongrowing Cells

Johan H. van Heerden *et al.*

Science **343**, (2014);
DOI: 10.1126/science.1245114

Lost in Transition: Start-Up of Glycolysis Yields Subpopulations of Nongrowing Cells

Johan H. van Heerden, Meike T. Wortel, Frank J. Bruggeman, Joseph J. Heijnen, Yves J. M. Bollen, Robert Planqué, Josephus Hulshof, Tom G. O'Toole, S. Aljoscha Wahl, Bas Teusink*

READ THE FULL ARTICLE ONLINE
http://dx.doi.org/10.1126/science.1245114

Cite this article as J. H. van Heerden *et al.*, *Science* **343**, 1245114 (2014).
DOI: 10.1126/science.1245114

Introduction: Cells use multilayered regulatory systems to respond adequately to changing environments or perturbations. Failure in regulation underlies cellular malfunctioning, loss of fitness, or disease. How molecular components dynamically interact to give rise to robust and adaptive responses is not well understood. Here, we studied how the model eukaryote *Saccharomyces cerevisiae* can cope with transition to high glucose levels, a failure of which results in metabolic malfunctioning and growth arrest.

Methods: We combined experimental and modeling approaches to unravel the mechanisms used by yeast to cope with sudden glucose availability. We studied growth characteristics and metabolic state at population and single-cell levels (through flow cytometry and colony plating) of the wild type and of mutants unable to transit properly to excess glucose; such mutants are defective in trehalose synthesis, a disaccharide associated with stress resistance. Dynamic ^{13}C tracer enrichment was used to estimate dynamic intracellular fluxes immediately after glucose addition. Mathematical modeling was used to interpret and generalize results and to suggest subsequent experiments.

Results: The failure to cope with glucose is caused by imbalanced reactions in glycolysis, the essential pathway in energy metabolism in most organisms. In the failure mode, the first steps of glycolysis carry more flux than the downstream steps, resulting in accumulating intermediates at constant low levels of adenosine triphosphate (ATP) and inorganic phosphate. We found that cells with such an unbalanced glycolysis coexist with vital cells with normal glycolytic function. Spontaneous, nongenetic metabolic variability among individual cells determines which state is reached and consequently which cells survive. In mutants of trehalose metabolism, only 0.01% of the cells started to grow on glucose; in the wild type, the success rate was still only 93% (i.e., 7% of wild-type yeast did not properly start up glycolysis). Mathematical models predicted that the dynamics of inorganic phosphate is a key determinant in successful transition to glucose, and that phosphate release through ATP hydrolysis reduces the probability of reaching an imbalanced state. ^{13}C-labeling experiments confirmed the hypothesis that trehalose metabolism constitutes a futile cycle that would provide proper phosphate balance: Upon a glucose pulse, almost 30% of the glucose is transiently shuttled into trehalose metabolism.

Discussion: Our work reveals how cell fate can be determined by glycolytic dynamics combined with cell heterogeneity purely at the metabolic level. Specific regulatory mechanisms are required to initiate the glycolytic pathway; in yeast, trehalose cycling pushes glycolysis transiently into the right direction, after which cycling stops. The coexistence of two modes of glycolysis—an imbalanced state and the normal functional state—arises from the fundamental design of glycolysis. This makes the imbalanced state a generic risk for humans as well, extending our fundamental knowledge of this central pathway that is dysfunctional in diseases such as diabetes and cancer.

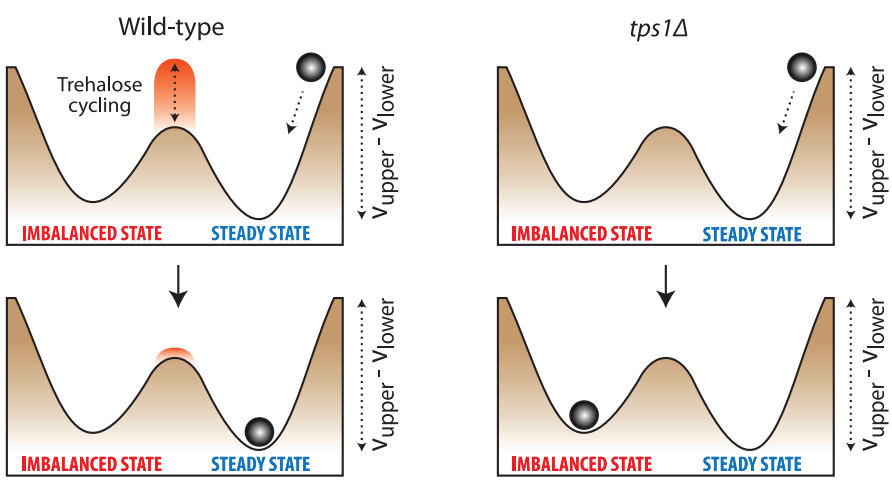

Initiation of glycolysis can have two outcomes. Upon glucose availability, glycolysis can end up in either a functional steady state or an unviable imbalanced state with imbalanced fluxes between ATP-consuming (V_{upper}) and ATP-producing steps (V_{lower}). In wild-type yeast, the transient activation of trehalose cycling pushes glycolysis toward the viable steady state. Failure to do so results in metabolic malfunctioning, as observed in mutants in trehalose biosynthesis (*tps1*Δ).

FIGURES IN THE FULL ARTICLE

Fig. 1. The coexistence of two glycolytic states underlies glucose-tolerant *tps1*Δ subpopulations.

Fig. 2. pH_i reveals distinct metabolic subpopulations.

Fig. 3. Metabolic subpopulations are caused by small variation in metabolic variables, and their sizes can be manipulated.

Fig. 4. Generalized core model of glycolysis can reach two stable, coexisting states.

Fig. 5. ^{13}C tracer enrichment reveals highly dynamic flux distributions through the trehalose cycle.

SUPPLEMENTARY MATERIALS

Supplementary Text
Figs. S1 to S18
Tables S1 to S8
References

The list of author affiliations is available in the full article online.
*Corresponding author. E-mail: b.teusink@vu.nl

Lost in Transition: Start-Up of Glycolysis Yields Subpopulations of Nongrowing Cells

Johan H. van Heerden,[1,2,3] Meike T. Wortel,[1,2,3] Frank J. Bruggeman,[1,3] Joseph J. Heijnen,[2,4] Yves J. M. Bollen,[3,5] Robert Planqué,[6] Josephus Hulshof,[6] Tom G. O'Toole,[7] S. Aljoscha Wahl,[2,4] Bas Teusink[1,2,3]*

Cells need to adapt to dynamic environments. Yeast that fail to cope with dynamic changes in the abundance of glucose can undergo growth arrest. We show that this failure is caused by imbalanced reactions in glycolysis, the essential pathway in energy metabolism in most organisms. The imbalance arises largely from the fundamental design of glycolysis, making this state of glycolysis a generic risk. Cells with unbalanced glycolysis coexisted with vital cells. Spontaneous, nongenetic metabolic variability among individual cells determines which state is reached and, consequently, which cells survive. Transient ATP (adenosine 5′-triphosphate) hydrolysis through futile cycling reduces the probability of reaching the imbalanced state. Our results reveal dynamic behavior of glycolysis and indicate that cell fate can be determined by heterogeneity purely at the metabolic level.

Key properties of biological systems are adaptability and robustness—the ability to maintain the physiological state in response to perturbations or dynamic conditions (*1*). Cells use multilayered regulation to respond adequately to changing environments or sudden perturbations. Failures in regulation underlie cellular malfunctioning, loss of fitness, or disease. In recent years, there has been a revived interest in metabolic processes, because many diseases are associated with metabolic aberrations, such as diabetes and cancer (*2*). Glycolysis is the central pathway in energy metabolism, which converts glucose to pyruvate with a net production of two adenosine 5′-triphosphate (ATP) molecules per glucose molecule. However, this net formation of ATP in "lower glycolysis" (Fig. 1) is preceded by an initial ATP investment at the first steps in the pathway ("upper glycolysis"; Fig. 1). This sequence of enzymatic steps in glycolysis, which is adopted by many organisms (*3*), implies a serious risk. If upper glycolysis outpaces lower glycolysis, a massive accumulation of glycolytic intermediates can occur with much reduced ATP production (*4*). This phenotype is observed in pancreatic β cells overexpressing glucokinase (coined acute glucose intolerance) (*5*), the enzyme that catalyzes the first step of glycolysis. Similarly, *Saccharomyces cerevisiae* mutants defective in the biosynthesis of the disaccharide trehalose, which branches off from glycolysis at the level of glucose-6-phosphate (G6P) (Fig. 1), show accumulation of the glycolytic intermediate fructose 1,6-bisphosphate (FBP) at low concentrations of ATP (*6*). We call this detrimental state of glycolysis an imbalanced state. We find that this imbalanced state is a risk also for normal cells. Through detailed system-level analysis of yeast glycolysis, we explain how phosphate dynamics is at the origin of the imbalance, and reveal how specific regulatory mechanisms affect the probability for cells to get trapped in it.

S. cerevisiae mutants with a defect in trehalose 6-phosphate (T6P) synthase (*tps1*), the first committed step in trehalose biosynthesis (Fig. 1), exhibit the imbalanced-state phenotype and are unable to grow on glucose (*7*). The molecular mechanism underlying this imbalanced phenotype has proven challenging to elucidate [we provide an extensive account of the literature in (*8*)]. T6P, the product of *tps1*, acts in vitro as a competitive inhibitor of the hexokinases (HXK1 and HXK2), with respect to glucose (*9*). This negative feedback loop was hypothesized to slow down the upper part of glycolysis and restore the balance in wild-type cells (*4*), but T6P-insensitive hexokinase mutants do grow on glucose (*10*). An alternative hypothesis assumes a reduced activity of glyceraldehyde-3-phosphate dehydrogenase (GAPDH) because of the low amounts of its substrate, cytosolic phosphate (P_i), in *tps1*Δ mutants. Accordingly, P_i release should enhance GAPDH activity and restore balance. In line with this hypothesis, enhanced glycerol production, which releases P_i, restores growth of *tps1*Δ mutants on glucose (*11*). Trehalose production from G6P also releases P_i (Fig. 1A); however, the capacity of trehalose synthesis was believed to be too low to provide enough P_i for the high flux of glycolysis (*12*).

We used a computational approach to better understand the complex phenotype of *tps1*Δ mutants. We adapted an existing kinetic model of glycolysis (*13*) by (i) introducing P_i as an explicit variable in the model (rather than as a fixed "commodity" metabolite) and (ii) allowing for the mobilization of P_i from vacuolar stores, based on in vivo nuclear magnetic resonance data that describe this behavior (*6*). The latter was necessary because the net accumulation of phosphate-containing glycolytic intermediates that are observed experimentally in the imbalanced state (Fig. 1B) is not possible without the import of P_i [details on these and other small adjustments to the original model are provided in (*8*)].

Two Glycolytic States Coexist

Simulations representing the *tps1*Δ mutant resulted in dynamic metabolite profiles that were qualitatively similar to experimentally observed profiles (Fig. 1B); that is, all metabolites were balanced, except for the intermediates between the upper and lower parts of glycolysis (Fig. 1B and fig. S3). Known experimental rescue mechanisms for the *tps1*Δ mutant, such as reduced activity of hexokinase (*14*) or enhanced glycerol production (*11*), could be reproduced in silico (figs. S11C and S14, C and D).

Our *tps1*Δ mutant model could reach another state, which resembled the wild-type steady state with proper flux, high ATP and P_i levels, and normal FBP levels. Whether this state was reached depended on the initial concentrations of the metabolites, as shown for FBP and P_i (Fig. 1B). Hence, two stable outcomes (states) coexisted in the model, a global steady state and an imbalanced state: the latter is a nontypical stable state, because some variables are not constant in time but rather accumulate. Other systems with more than one stable state, as found in sporulation (*15*) or differentiation (*16*), often result in phenotypically different subpopulations in an isogenic population. We assessed experimentally whether we could find evidence for such subpopulations as well, by asserting that only the functional glycolytic state would support growth. On the basis of serial dilution plating of wild-type and *tps1*Δ cultures on galactose and glucose (*8*), we estimated that about 1 in 10^3 to 10^4 *tps1*Δ cells grew on excess glucose (Fig. 1C). This small subpopulation size is consistent with the very long lag phase we observed in glucose liquid cultures (Fig. 1D). In the past, glucose-positive *tps1*Δ colonies were usually discarded as revertants or rescue mutants. However, when *tps1*Δ colonies were directly picked from glucose plates and subjected to another transition via galactose to glucose, the original subpopulation structure with less than

[1]Systems Bioinformatics/Amsterdam Institute for Molecules, Medicines and Systems (AIMMS)/Netherlands Institute for Systems Biology, VU University, De Boelelaan 1085, 1081 HV Amsterdam, Netherlands. [2]Kluyver Centre for Genomics of Industrial Fermentation/Netherlands Consortium for Systems Biology (NCSB), Delft University of Technology, Julianalaan 67, 2628 BC Delft, Netherlands. [3]Department of Molecular Cell Biology, VU University, 1081 HV Amsterdam, Netherlands. [4]Department of Biotechnology, Delft University of Technology, 2628 BC Delft, Netherlands. [5]LaserLaB Amsterdam, VU University, 1081 HV Amsterdam, Netherlands. [6]Department of Mathematics, VU University, 1081 HV Amsterdam, Netherlands. [7]Department of Molecular Cell Biology and Immunology, Vrije University Medical Center, v/d Boechorststraat 7, 1081 BT Amsterdam, Netherlands.

*Corresponding author. E-mail: b.teusink@vu.nl

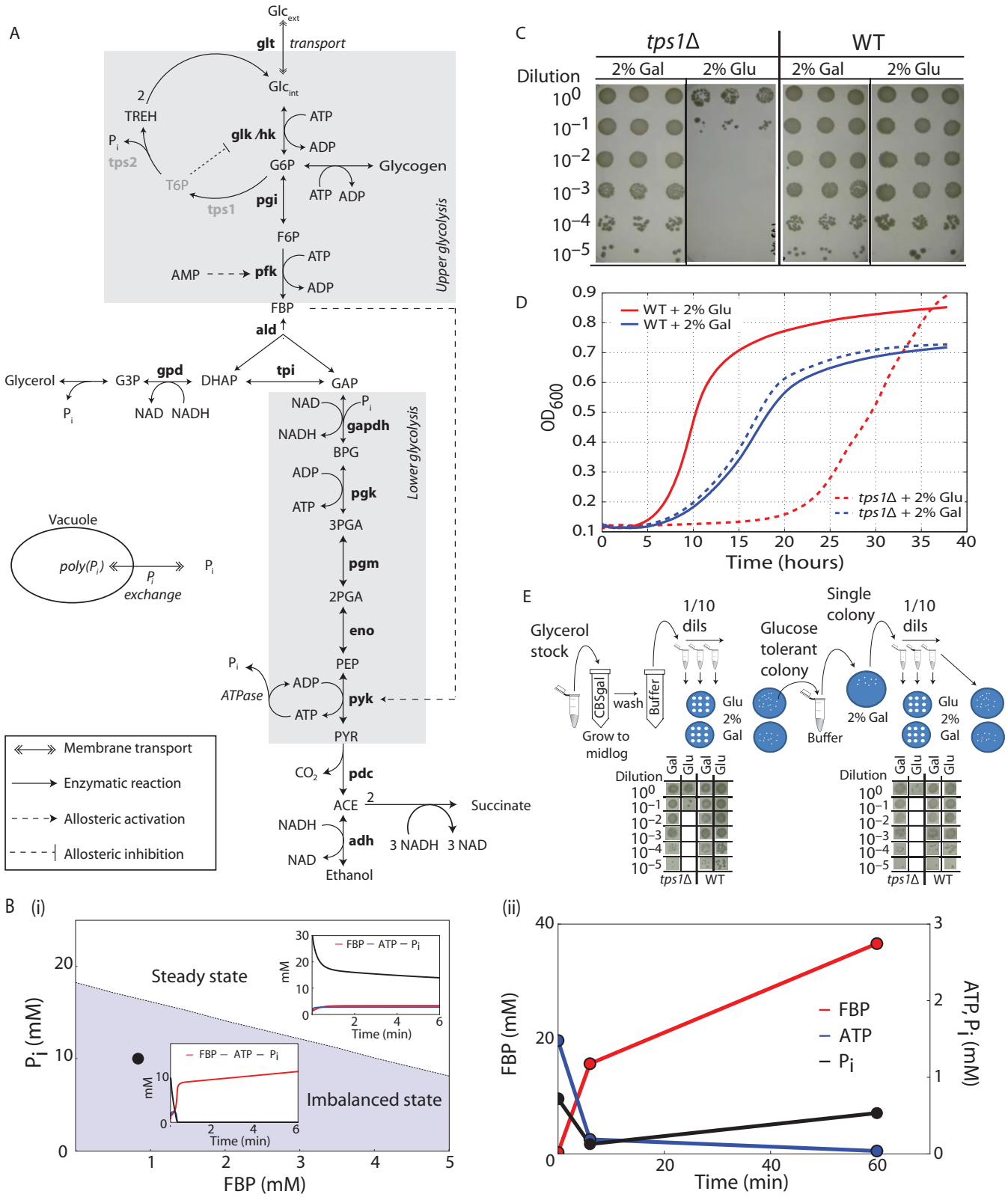

Fig. 1. The coexistence of two glycolytic states underlies glucose-tolerant *tps1*Δ subpopulations. (**A**) Schematic illustration of glycolysis and the trehalose cycle. (**B**) Depending on initial conditions, the *tps1*Δ-like model can reach one of two stable states. (i) Normal steady state (white area) or an imbalanced state (gray area). The black circle indicates the initial values for P_i and FBP used (table S2). (ii) Simulation of the imbalanced state is qualitatively similar to experimentally observed profiles [data reproduced from (*9*)]. (**C**) Serial dilution plating reproducibly shows glucose-tolerant subpopulations of between 1 in 10^3 and 1 in 10^4 *tps1*Δ cells ($n = 3$). (**D**) Growth curves for wild type (WT) and *tps1*Δ on glucose (Glu) and galactose (Gal): Glu *tps1*Δ cells show extended lag phase as a consequence of a large nongrowing background. (**E**) Summary of the propagation scheme and a representative result (see fig. S5C for full scheme) show that glucose tolerance can be reset, because populations derived from a glucose-tolerant colony exhibit subpopulation structures similar to initial populations derived from glycerol stocks.

1 in 10^3 glucose-tolerant colonies was restored (Fig. 1E and fig. S5C). This argues against a genetic basis. We therefore conclude that there is a small subpopulation of glucose-positive *tps1*Δ cells that arises from spontaneous phenotypic—as opposed to genetic—variability.

We reexamined the reported inhibitory effect of low concentrations of glucose on *tps1*Δ mutant growth in the presence of excess galactose (*17*). Plating experiments again showed that the growth inhibition observed at the population level is in fact caused by a glucose-dependent increase in the size of a subpopulation that was unable to grow (fig. S6A). A simple mathematical model of population growth dynamics with different growing and nongrowing subpopulation sizes (*8*) reproduced the experimental data (*17*) very well (fig. S6B).

Intracellular pH Reveals Two Metabolic Subpopulations

To visualize the two subpopulations, we made use of the observation that *tps1*Δ mutants, when exposed to glucose, are unable to maintain pH homeostasis because they produce too little ATP (*6*). Hence, after glucose addition, the intracellular pH (pH_i) of *tps1*Δ populations decreased by more than 1 pH unit compared to that of wild-type cells (Fig. 2A). After confirming that different subpopulations could be distinguished on the basis of pH_i signals (Fig. 2B), we used flow cytometry as a high-throughput approach to study the structure of both *tps1*Δ and wild-type populations exposed to galactose and glucose. We found two subpopulations of *tps1*Δ cells of sizes that agreed with the plating assays and growth lag phases (Fig. 2C). We also tested wild-type cells because analysis of the wild-type version of the model also showed two stable states (fig. S4). Indeed, a subpopulation of wild-type cells with low pH appeared in cultures exposed to glucose, but a similar response was observed for galactose (Fig. 2C). The size of the subpopulation, about 7%, was larger than the model suggested (but not unexpectedly; fig. S4). These results indicate that the imbalanced state is a general property of glycolysis that cannot be fully prevented by regulatory mechanisms operative in wild-type cells.

Metabolic Variability Determines State of Glycolysis

We tested in silico whether the observed phenotypic variability in the response to sugar addition could be reproduced by introducing spontaneous variation in enzyme and initial metabolite concentrations. We sampled these concentrations from Gaussian distributions with realistic coefficients of variation (*18*). The mean of the initial metabolite concentrations was based on metabolite data for wild-type cells grown on galactose (*19*), the sugar on which we grew *tps1*Δ before glucose addition. We generated 10^6 *tps1*Δ-like models each with unique initial conditions and simulated a galactose-to-glucose transition. Less than one in a thousand models actually reached a functional steady state. Thus, heterogeneity in the amounts of glycolytic enzymes and metabolites appears to cause some cells to survive glucose dynamics, whereas others do not. This is striking, because metabolism is often considered to operate in a deterministic regime due to rather high concentrations of enzymes and intermediates. Phenotypic variation by nongenetic variability is usually studied in genetic circuits that naturally operate at a stochastic regime with low copy numbers for key components (*20*).

It is relevant to compare the above observations with frameworks such as fluctuation-induced bistable switching (*21*, *22*), which has previously been linked to the emergence of phenotypic heterogeneity. In contrast to such stochastic switching phenomena, the emergence of the two distinct phenotypes (viable and nonviable) described here does not depend on the coexistence of two qualitatively different physiological states before a glucose perturbation. Our interpretation of the above data is that spontaneous, nongenetic variation between cells creates a continuous probability distribution for metabolite concentrations and metabolic fluxes. Within the space of these initial physiological states, a subspace exists that characterizes the cells that survive a sudden glucose excess exposure (fig. S7) (*8*).

To assess which parameters and initial conditions most affect the probability to reach an imbalanced or functional steady state, we performed a linear discriminant analysis over all our model simulations (*8*). A single discriminant accounted for 99% of the differences in initial conditions that lead to either the balanced or imbalanced states

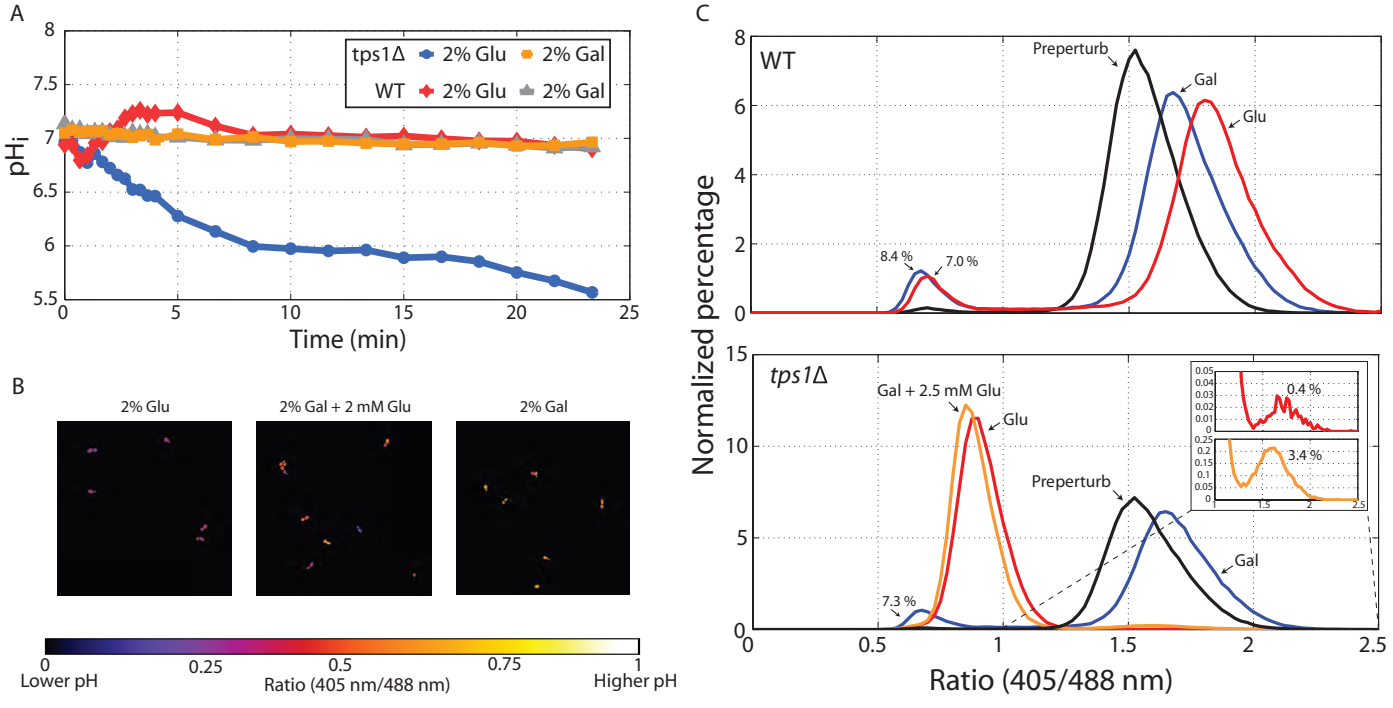

Fig. 2. pH_i reveals distinct metabolic subpopulations. (**A**) Population-level pH_i responses show the disruption of pH homeostasis of *tps1*Δ cells in response to 2% glucose. After a 2% glucose or galactose pulse, the pH_i of WT and *tps1*Δ populations is shown in time. (**B**) Fluorescence microscopy shows that distinct metabolic states can be visualized using pH_i readouts. (**C**) Flow cytometry measurements based on pHluorin signals reveal the presence of distinct subpopulations in both WT (top graph) and *tps1*Δ populations (bottom graph) after perturbations with glucose and galactose (black, preperturbation sample in wash buffer; blue, 2% Gal; red, 2% Glu; orange, 2% Gal + 2.5 mM Glu).

(fig. S11A). This discriminant identified parameters and initial metabolite concentrations that tend to either reduce the flux through the upper part of glycolysis or enhance the flux through lower glycolysis (Fig. 3A). The parameters related to the primary mechanisms known to rescue the *tps1*Δ mutant phenotype (*23*) were all represented.

Size of Subpopulations Can Be Manipulated

We looked for ways to experimentally influence the size of the two subpopulations. Respiratory inhibitors, in particular antimycin A (*24*), have been shown to improve growth in the presence of glucose. However, ethanol, the solvent of antimycin A, produced pronounced decreases in the lag phase (Fig. 3B), completely dominating the antimycin A effect (fig. S5D). These results were confirmed by plating assays (fig. S6C) and flow cytometry measurements of pH_i (fig. S9) (*8*). We repeated the in silico random sampling approach at different ethanol concentrations and reproduced the positive effect of ethanol (Fig. 3C). The model showed that the increase in ethanol concentration increased P_i release through glycerol formation (fig. S11B) driven by an increased NADH (reduced form of nicotinamide adenine dinucleotide)/NAD (oxidized form of nicotinamide adenine dinucleotide) ratio (*25*). This model prediction was experimentally tested in *tps1*Δ mutant cultures by the addition of formate. Although formate cannot be used as a carbon source by yeast, its conversion to CO_2 by formate dehydrogenase (*26*) enhances NADH formation. Indeed, formate additions similarly decreased the lag phase, implying a NADH-driven increase in glycerol production that subsequently increases the proportion of *tps1*Δ cells in the population that could grow on glucose (fig. S5E).

Core Model Explains and Generalizes Dynamics

To generalize our findings and to provide a deeper understanding of the observed coexistence of two stable states, we captured the essential features of the large model in a reduced model. This generalized core model (*8*) only considers the concentrations of FBP, ATP, and P_i and four reactions: (i) a lumped upper glycolysis reaction (v_{upper}), (ii) a lumped lower part of glycolysis (v_{lower}), (iii) an ATP-demand reaction (v_{ATP}), and (iv) a P_i import or export reaction (v_P) (Fig. 4). Detailed mathematical analysis showed that such a generalized glycolytic pathway has two stable states representing a functional steady state and an imbalanced state.

Figure 4 shows the system dynamics that lead to these two states: The difference between the left and right panel is only the initial P_i level (10.4 and 9.4 mM, respectively). How can the different outcomes in these simulations be explained? At the start of the simulation (when glucose is added), $v_{upper} > v_{lower}$, and this difference causes the concentration of the intermediate FBP to increase (as $dFBP/dt = v_{upper} - v_{lower}$). For a balanced steady state, v_{lower} needs to accelerate to equal the rate of v_{upper} (note that this challenge becomes bigger if the activity of v_{upper} is higher). P_i is the phosphate source for FBP, and therefore, FBP accumulation results in a drop in P_i (Fig. 4). Because both FBP and P_i are substrates of v_{lower}, the accumulation of FBP stimulates v_{lower}, whereas the drop in P_i tends to slow it down: Which effect is dominant may determine the fate of the system. If P_i is high initially, a drop in P_i will not affect v_{lower} and the FBP increase will dominate, resulting in the functional steady state being reached (Fig. 4, left panel). Similarly, if P_i is liberated quickly enough directly by storage/uptake (v_P) or indirectly by ATP hydrolysis (v_{ATP}), P_i will drop less quickly and the balanced steady state can also be reached. If, however, P_i is low at the onset of glucose addition or P_i mobilization is too slow, or both, the decrease in P_i will quickly become a limiting factor for v_{lower} and will dominate the stimulating effect of accumulating FBP. In this case, v_{lower} will not accelerate quickly enough to reach the rate of v_{upper}, and the system will collapse to the imbalanced state (Fig. 4, right panel). Once in this imbalanced state, continuous P_i mobilization from uptake or storage paradoxically maintains the imbalance. In this low P_i, low ATP state, imported P_i enhances the rate of v_{lower}, but the concomitant production of ATP will increase v_{upper} two times more (due to the stoichiometric coupling of ATP in glycolysis; Fig. 4B). Hence, the imbalance and, thus, FBP accumulation will only get bigger with faster P_i import, as observed in the core model and the detailed model (fig. S1).

Trehalose Metabolism Constitutes Transient Futile Cycling

The core model predicted that enhanced P_i mobilization through ATP hydrolysis by v_{ATP} could enlarge the set of initial conditions that leads to a functional steady state, or could even result in the disappearance of the imbalanced state altogether (fig. S14). This was confirmed in the detailed model. We realized that, in yeast, the full trehalose cycle (Fig. 1A) could act as a mechanism for ATP hydrolysis through futile cycling. This cycling of trehalose should be able to remove the existence of the imbalanced state or at least reduce the probability to reach it, providing a rationale why trehalose metabolism affects glycolytic function.

To estimate the dynamic fluxes through the trehalose network upon a transition to glucose excess, we used a dynamic ^{13}C-labeling approach (*8*). Wild-type cells were grown in a glucose-limited chemostat and treated with either 110 mM [^{12}C] glucose or uniformly labeled [U-$^{13}C_6$]glucose pulses. The time course of the concentrations and the average carbon labeling enrichments for key intermediates are shown in Fig. 5A. For most metabolites, up to full enrichment was achieved very rapidly; in contrast, the large trehalose pool was enriched to only 14% at the end of the experiment. From these data, the flux of glucose through the different glycolytic enzymes was estimated on the basis of a hybrid modeling approach (*27*). The flux profiles indicated that (i) fluxes changed rapidly after a glucose pulse, at similar time scales as key metabolites, such as ATP (Fig. 5B); (ii) fluxes through TPS1 and TPS2 increased and subsequently decreased between 0 and 5 min; and (iii) at its maximum, as much as 28% of the glucose taken up was branched into trehalose (Fig. 5C). The transient nature of the flux through the trehalose pathway is consistent with the existence of two stable states in glycolysis, that is, once the system has reached the viable steady state, the need for excessive ATP hydrolysis through futile trehalose cycling has disappeared. Thus, we suggest that trehalose cycling constitutes a transient futile

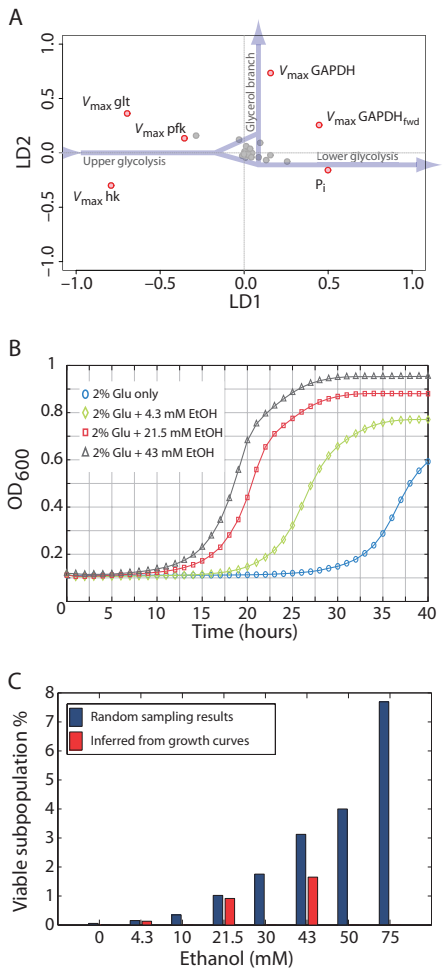

Fig. 3. Metabolic subpopulations are caused by small variation in metabolic variables, and their sizes can be manipulated. (**A**) Linear discriminant analysis of randomly sampled initial conditions (metabolites and V_{maxes}) highlights the variables that most significantly affect the probability of reaching either the normal steady state or the imbalanced state. (**B**) In liquid cultures, lag phases of *tps1*Δ cultures decreased with increasing concentrations of ethanol (EtOH) in the medium. (**C**) The positive effect of ethanol as percentage of viable cells [experimental data: red bars (*8*)] can be reproduced by a population of models with initial conditions sampled from a Gaussian distribution as described in the main text (blue bars).

cycle, large enough to push the system's dynamics into the functional steady state.

Different Mechanisms Contribute to Robustness

Finally, we examined the contribution of various aspects of trehalose metabolism to establish proper glycolytic functioning, through random sampling of initial conditions in the full kinetic model (Fig. 5D). Whereas the combined trehalose cycling and negative (T6P-mediated) feedback on hexokinase resulted in 100% viability in the wild-type version of the model, apparent futile cycling of trehalose alone resulted in a regular steady state in 76% of the sampled cases. Removal of G6P without P_i release (only possible in silico) resulted in a functional state in 4% of the cases. This shows that phosphate recovery is the primary safety mechanism, with hexokinase inhibition also contributing. The reported inhibition of trehalose synthesis by P_i (*28*) reinforces this picture, because low P_i concentrations will relieve inhibition and ensure P_i mobilization. These results provide a strong basis for the interpretation of population-level phenotypes of various mutants in trehalose metabolism and hexokinase (*8*).

Start-Up of Glycolysis Requires Dynamic Regulation

From our work, a dynamic picture emerges where the organization of glycolysis in ATP-investing upper and ATP-producing lower parts provides a major challenge for robust start-up upon activation. After environmental changes (for example, nutrition, hormone, and drug), proper steering through a dynamic landscape consisting of undesired states requires specialized regulatory mechanisms. Our work shows that phosphate dynamics is an essential determinant of the state that is reached. Because existing glycolytic models ignored P_i dynamics, the coexistence of two states in glycolysis was not previously discovered.

The core model demonstrated that mostly generic features of glycolysis give rise to this two state outcomes, in particular, (i) its stoichiometry in ATP consumption and production, and (ii) the (universal) equilibrium constants of phosphofructokinase (large; allowing accumulation of FBP) and GAPDH (small; requiring high P_i levels to drive the reaction). In yeast, trehalose metabolism apparently provides protection against the imbalanced state, albeit not 100% fail-safe based on flow cytometry (Fig. 2C); the observed failure of wild type (~7%) could reflect a trade-off between different aspects of the transition to high sugar, because a higher success rate will require tighter regulation or higher futile cycling that will make start-up slower or more costly, respectively.

Other systems, notably mammalian cell types, have adopted alternative mechanisms that may function to prevent glycolytic imbalance. In human cell types, feedback inhibition of hexokinase or glucokinase, either by the product G6P (muscle) or a glucokinase regulatory protein (liver), is a well-known regulatory mechanism for glycolysis (*29*). Pancreatic β cells seem to have no protective mechanism, but have low glucokinase activity

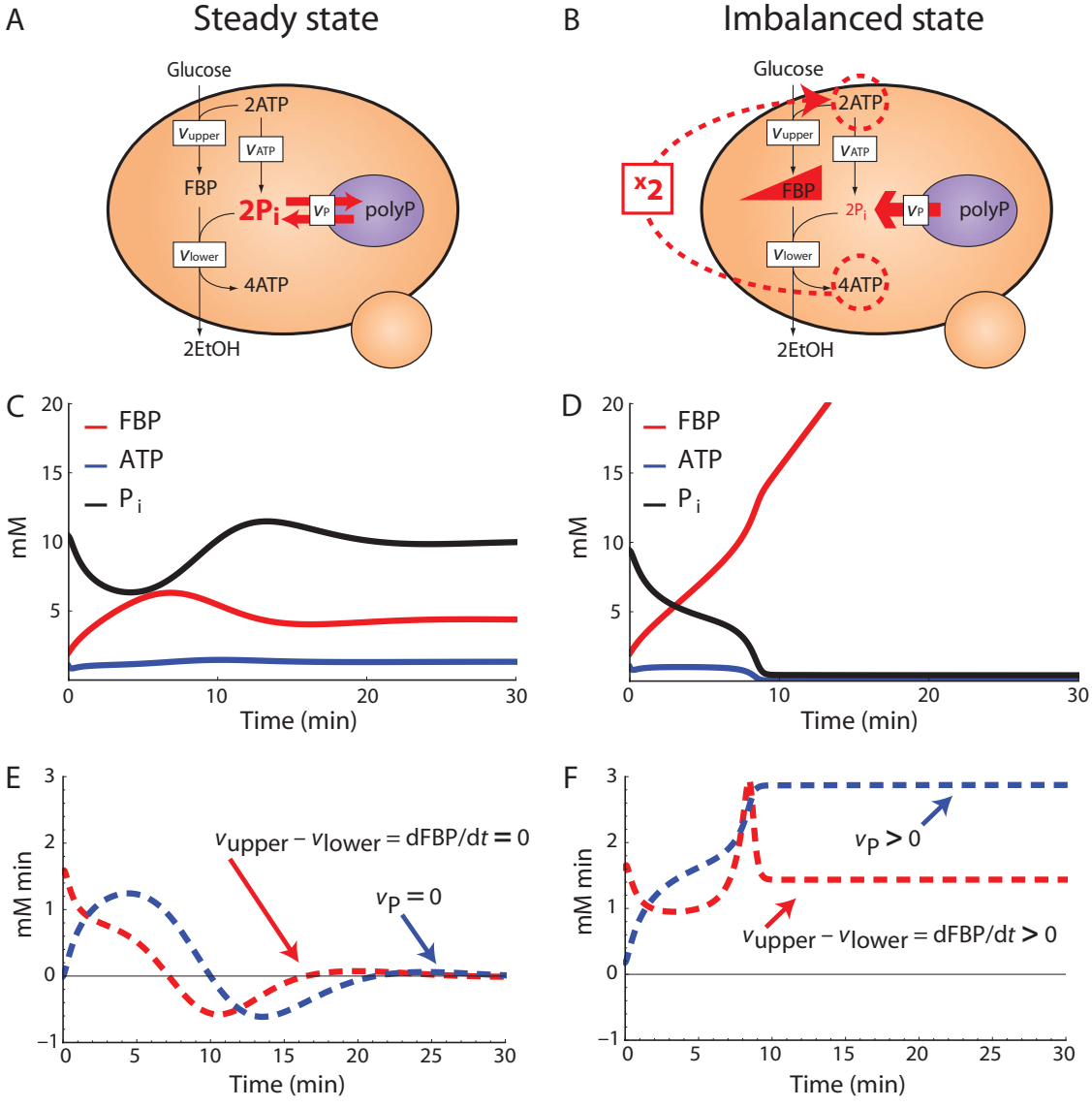

Fig. 4. Generalized core model of glycolysis can reach two stable, coexisting states. The left panel shows the global steady state, and the right panel the imbalanced state. The difference between panels is the initial P_i level (10.4 and 9.4, respectively). (**A** and **B**) Stoichiometry of the core model, with red arrows emphasizing the vacuolar flow of P_i from polyphosphates (polyP). The coupling between the upper and lower part of glycolysis through ATP is emphasized by the red dashed line (B). (**C** and **D**) Metabolite levels for a simulation of the core model, resulting in steady state (metabolite levels constant in time) (C) or imbalance (FBP accumulation at very low P_i and ATP levels) (D). (**E** and **F**) Characteristic rates that specify the states: The red dashed lines indicate the difference in rate between upper and lower glycolysis ($v_{upper} - v_{lower}$), which is zero at steady state (E) and is positive at the imbalanced state (F). The dashed blue lines represent the vacuolar import rate of P_i (v_P), which should be zero at steady state. In (F), the constant positive v_P indicates mobilization of P_i, which sustains accumulation of FBP (red dashed line) through the stoichiometric coupling of ATP.

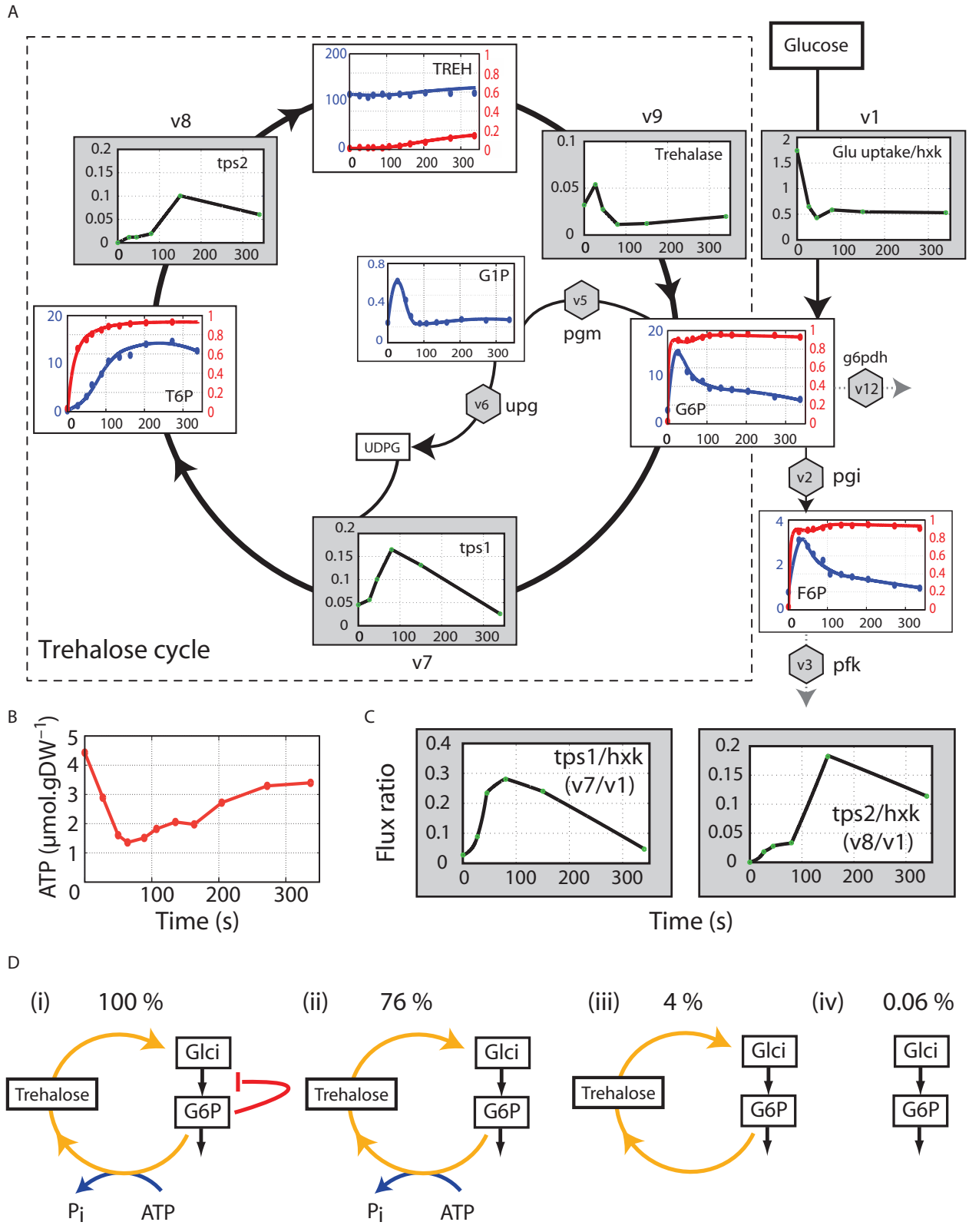

Fig. 5. ^{13}C tracer enrichment reveals highly dynamic flux distributions through the trehalose cycle. (**A**) Selection of data [complete data set in (*8*)] superimposed on the trehalose cycle. White boxes contain metabolite data, with concentrations (µmol gDW^{-1}) in blue and tracer enrichment (fraction) in red (symbols represent measurements, and lines represent model fits); *x* axes show time in seconds. Gray boxes show flux profiles (µmol gDW^{-1} s^{-1}) of the indicated reactions in time (s). (**B**) ATP concentration profile shows a response time similar to that of flux channeling toward the trehalose pool via the tps1 reaction. (**C**) Dynamic flux ratios of tps1 (v7) and tps2 (v8) relative to hxk (v1) show that up to 28% of glucose is dynamically routed into trehalose metabolism. (**D**) Percentage of balanced steady states found with randomly sampled initial conditions as input for different features of the trehalose cycle. Different aspects of trehalose metabolism contribute to the overall probability to reach the functional steady state.

that would prevent the upper part of glycolysis from being too fast. Upon overexpression of hexokinase, these cells exhibit a similar metabolic imbalance to that observed in yeast *tps1*Δ mutants (*5*), providing relevance for this state in mammalian metabolism.

Our findings have major implications for biotechnological applications and disease. In biotechnology, poor mixing in large-scale fermenters causes dynamic conditions, which—often in combination with genetic manipulations—may create conditions in which individual cells behave very differently from the measured population average. In disease, cancer in particular, the regulation of glycolysis has recently regained great interest because of the Warburg effect, characterized by an enhanced glycolytic flux and lactate production (*30*). Our work provides systems-level insight into the dynamic regulation of glycolysis. As an example, feed-forward activation of pyruvate kinase (PK) by FBP is impaired in the PKM2 splice variant that replaces the original PKM1 protein in many cancer cells (*31*). Such feed-forward activation of PK by FBP, observed from bacteria to man, could act as an additional safety mechanism to prevent a metabolic imbalance in glycolysis: FBP activation would help to accelerate the lower part of glycolysis if FBP starts to accumulate. Indeed, in all our models, removing the positive feedback on PK enhanced the probability to reach imbalance. Intriguingly, PKM2 expression in tumors coincides with an alternative phosphoglycerate mutase activity that instead of ATP produces P_i from PEP (*32*). Such an activity would fit with the role of P_i release to ensure robust functioning of glycolysis. Interfering with protective mechanisms against the metabolic imbalance state in tumor cells, or perhaps, counterintuitively, enhancing glucose uptake rather than inhibiting it, may provide a rationale for sophisticated treatment strategies.

Materials and Methods

Strains, Media, and Growth Conditions

All strains used in this study are listed in table S3. The *S. cerevisiae* strains based on the BY4743 background were used to characterize growth behavior and subpopulation dynamics. The W303-1A background was used to evaluate the effects of HXK2 overexpression. All growth experiments were performed at 30°C using a defined mineral medium [see (*33*) for reference] with required amino acid supplements, buffered to pH 5 (30 mM sodium citrate/citric acid buffer) and supplemented with either 2% galactose (CBS-Gal) or 2% glucose (CBS-Glu), with additions as indicated. Defined mineral medium plates were made by addition of 1% agarose to the growth medium. Plates were always incubated for 3 days at 30°C before counting colonies, unless stated otherwise. Medium lacking a carbon source (CBS-C) was used as a wash and resuspension buffer throughout.

For ^{13}C tracer experiments, the haploid prototrophic *S. cerevisiae* strain CEN.PK 113-7D (*34*) was cultured in an aerobic glucose-limited chemostat using a low-salt defined medium (*35*) containing the following: glucose (8.25 g/liter), ethanol (0.39 g/liter), and silicone antifoaming agent (0.05 g/liter) (BDH Chemicals), yielding a steady-state biomass concentration of 4.0 g_{DW}/liter. Ethanol was added to suppress spontaneous oscillations (*36*). The continuous culture was performed in a 7.0-liter bioreactor with 4.0-liter working volume (Applikon) at a dilution rate of 0.1 per hour. Temperature was set to 30°C, and pH was kept constant at 5.0 by automated addition of 4.0 M KOH (aq). Air was sparged through the culture at a rate of 2.0 liter/min, and stirring was set to 800 rpm. Steady-state conditions were assumed when, after five volume changes, dissolved oxygen, off-gas composition, and biomass concentration were stable. Biomass dry weight was measured, in triplicate, by filtering 5.0-ml broth samples on preweighed and predried 0.45-μm cellulose membranes (Supor 450, Gelman Sciences). Next, the membranes were washed with 10.0 ml of demineralized water and placed at 70°C to dry (24 hours), before being weighed.

Strain Constructions

All yeast transformations were performed according to (*37*). The pYES-PACT1-pHluorin plasmid described in (*38*) was supplied by G. Smits. The plasmids for HXK2 overexpression described in (*39*) were supplied by J. Thevelein.

Microtiter Growth Experiments

Growth behavior in response to different carbon sources and various perturbing agents was monitored using 96-well microtiter plates. All inoculums, unless stated otherwise, were derived from single colony isolates. Glycerol stocks were streaked out onto YEP + 2% galactose agar plates (1% yeast extract, 2% peptone, 2% agar) and incubated at 30°C. After 2 to 3 days, single colonies were isolated directly from the plates and resuspended in CBS-C. Optical densities (OD_{600}) were adjusted to be in the order of 0.1. Each suspension (biological replicate) was divided such that it could be subjected to all permutations within a single experiment. Once carbon sources and, where applicable, perturbing agents were added, microtiter wells were filled with 300 μl of prepared culture, and growth was monitored at 600 nm, using either a SpectraMax Plus384 (Molecular Devices) or a Multiskan GO (Thermo Fischer Scientific) microplate spectrophotometer. All experiments were done with at least two biological replicates per condition. All growth profiles are presented as the average of biological replicates, unless stated otherwise.

^{13}C Tracer Enrichment Experiment and Trehalose Cycle Flux Estimations

Glucose Pulse Perturbations

Glucose pulse perturbations were performed by coupling a BioScope reactor (*36*) to the chemostat culture; this facilitated multiple sequential perturbations without disturbing the steady-state reference culture in the chemostat. The BioScope flow was calibrated to a rate of 0.475 ml/min, which allowed for a total sampling time of 5 min 37 s with samples after −0, 27, 50, 64, 89, 107, 135, 163, 204, 272, and 337 s. The culture was perturbed by the addition of 110 mM glucose to the broth flow when entering the BioScope (see fig. S15 for an illustration of the experimental setup). The sampling time was chosen on the basis of a priori expectations of flux dynamics through central carbon metabolism and represents a trade-off between resolving rapid and slow enrichments of the various metabolite pools. Within our system, the main challenge was to ensure that the tracer was sufficiently propagated to the large trehalose pool while maintaining some degree of resolution for the much smaller and rapidly labeled upper glycolytic metabolite pools. The experiments were performed in duplicate from the same chemostat culture for both glucose perturbation (for concentration measurements) and a perturbation with uniformly labeled ^{13}C [U-$^{13}C_6$]glucose (for labeling enrichment measurements).

Sample extractions, processing, and analysis were performed as in (*35*) and were briefly described below.

Metabolite Extraction and Sample Storage

Tubes with 100% methanol (5 ml) were taken from the cryostat (−40°C), and 1 ml of broth was sampled directly into this quenching solution. The biomass is separated from the quenching solution by centrifugation. To remove the broth supernatant, an additional washing step is included. In the case of concentration measurements, ^{13}C extract was added. The washed pellet is then extracted by the addition of 5 ml of 75% (v/v) boiling ethanol. Samples were immediately vortexed and placed in a water bath at 95°C for 3 min and then returned to the cryostat. Ethanol was evaporated using a RapidVap N2 (Labconco). The dried residues were stored at −80°C until further processing.

Metabolite Concentration and Mass Isotopomer Quantifications

Mass isotopomer fractions—as well as concentrations of G6P, fructose 6-phosphate (F6P), glucose 1-phosphate (G1P), FBP, T6P, uridine diphosphoglucose (UDP-glucose), and 6-phosphogluconate (6PG)—were determined using anion exchange liquid chromatography–tandem mass spectrometry (LC-MS/MS) (*35*). The concentration of ATP was determined by ion-pair reversed-phase LC-MS/MS (*35*). Additionally, G6P, F6P, FBP, T6P, and trehalose were measured, as methoxime-trimethylsilyl derivatives, by gas chromatography–MS. The intracellular concentrations were determined on the basis of isotope dilution mass spectrometry (*35*). Where applicable, metabolite values determined by more than one platform were combined.

Hybrid Modeling Approach

The estimation of intracellular fluxes based on the concentration and ^{13}C enrichment data was

performed according to the procedure outlined by (*27*). A definition of the network with indicated C atom transitions that was used to automatically generate the concentration and labeling enrichment balances is shown in table S8; the notation introduced by (*40*) was used. Figure S16 provides a graphical illustration of reactions and metabolite pools included in our analysis.

Population-Level pHluorin Measurements

pHluorin-transformed cells (*38*) (see table S3) were inoculated into CBS-Gal and grown overnight to an OD_{600} of 0.8 to 1. Cells were collected by centrifugation, washed twice with ice-cold CBS-C, and resuspended to an OD_{600} of about 1. Cell suspensions (200 µl) were transferred to black polystyrene clear-bottom 96-well microtiter plates (Greiner Bio-One), and pHluorin fluorescence emission was measured at 510 nm using an Omega FLUOstar microtiter plate spectrofluorometer (BMG LABTECH GmbH), with excitation bands of 10 nm centered about 390 and 470 nm, respectively. Glucose was added to a final concentration of 2% by automated injection. Additionally, pHluorin signals were collected for cultures growing on 2% galactose (OD_{600} ~0.8).

Calibration curves were constructed exactly as described in (*38*). Background fluorescence for a wild-type culture not expressing pHluorin was measured in triplicate and subsequently subtracted from all measurements. The background-corrected ratio of emission intensity ($Em510_{390ex}/Em510_{470ex}$) was converted to pH by a function derived from the constructed calibration curve.

pHluorin Microscopy

Sample Preparation and Data Acquisition

*Tps1*Δ cells were grown to an OD_{600} of about 0.8. Cells were harvested by centrifugation at 4000 rpm for 5 min and washed twice in CBS-C. Samples were resuspended in CBS-C to an OD_{600} of about 1 and kept on ice until the addition of carbon sources. After addition of either 2% glucose, 2% galactose, or 2% galactose + 2 mM glucose, cells were incubated on a shaker for 30 min at 30°C, whereas microscope slides were prepared with 1% agarose pads. Agarose was dissolved in CBS-C. Once set, 20 µl of cell culture was pipetted directly onto the agarose and sealed with a cover slip and VALAP (a mixture of equal amounts of Vaseline, lanolin, and paraffin wax).

pHluorin fluorescence images were collected on a Nikon Ti-E inverted microscope using a CFI Plan Apochromat 60× oil immersion objective (Nikon Instruments). pHluorin was excited using either a 30-mW, 405-nm diode laser or a 90-mW, 488-nm diode laser from an Agilent MLC400 laserbox (Agilent Technologies). Both lasers were attenuated to 7% of their maximal power using an acousto-optical tunable filter. Emission light was selected using a 525-nm filter with 45-nm band width (Semrock) and recorded on a cooled back-illuminated electron-multiplying (EM) charge-coupled device camera (iXon DU897, Andor) using exposure times of 100 ms and an EM gain of 100 V.

Image Processing and Data Analysis

Images were processed and analyzed using ImageJ version 1.45s (*41*). General background correction was applied by the built-in function, with a rolling ball radius of 50 pixels and smoothing enabled. False-color images were generated from the ratio of emission intensities resulting from excitation at 405 and 488 nm ($Em525_{405ex}/Em525_{488ex}$).

pHluorin Flow Cytometry

Sample Preparation and Perturbation

Wild-type and *tps1*Δ cells were cultured, harvested, washed, and resuspended as described for above for microscopy. Carbon sources (wild type: 2% Glu or 2% Gal; *tps1*Δ: 2% Glu, 2% Gal or 2% Gal + 2.5 mM Glu) were added about 45 min before data acquisition. In addition, signals for cells suspended in CBS-C (unperturbed) were also collected about 45 min after resuspension.

A second set of experiments was performed to evaluate whether the presence of ethanol leads to the enrichment of the functional steady-state fraction of a *tps1*Δ population when challenged with glucose. Single colonies were picked directly from a galactose plates and resuspended in CBS-C. Suspension was perturbed as before, with either 2% Glu, 2% Gal, 2% Glu + 40 mM ethanol, or 2% Gal + 1 mM Glu. Samples not expressing pHluorin were always included to estimate background fluorescence signals.

Data Acquisition

Flow cytometry data were acquired on a CyAn ADP 9 Color flow cytometer (Beckman Coulter). pHluorin was excited by a 50-mW, 405-nm laser and a 25-mW solid-state 488-nm laser, respectively, and emission was detected through a 530/40-nm filter. Laser voltages were set at a minimum value that displayed the entire unperturbed wild-type population on a linearly scaled bivariate plot. The acquisition limit was 10^6 events per sample.

Data Analysis

Raw data files (.fcs) were processed and analyzed using MATLAB R2012b. Data were extracted from FCS (flow cytometry standard) files using the fcsread.m function, available in the MATLAB File Exchange repository (www.mathworks.nl/matlabcentral/fileexchange/8430-flow-cytometry-data-reader-and-visualization/content/fcsread.m). The channel-specific average background values were calculated from samples not expressing pHluorin and subtracted from each individual data point. In the first set of experiments (Fig. 2C), this threshold was 25 times the channel-specific background signal, and for the second set of experiments (fig. S9), this was 5 times the channel-specific background signal. This difference is a consequence of lower overall signal in the second set of experiments. The chosen thresholds resulted in an average of about 200,000 events being retained for each sample, in both experiments.

Fluorescence signals for each event were calculated as the ratio of emission intensity resulting from excitation at 405 and 488 nm ($Em530_{405ex}/Em530_{488ex}$). Frequency data (bins = 101) for each sample were normalized to sample-specific total post-filter events and expressed as percentages.

Kinetic Modeling

All models were implemented and analyzed using Mathematica 9.0 (Wolfram Research). The time simulations were performed with the NDSolve function. A steady state is defined as a state, characterized by the metabolite concentrations, where all time derivatives of internal metabolite concentrations are equal to zero. Steady states were calculated by solving these equalities with the FindRoot function. Metabolite concentrations from the time simulations, after 250 simulation minutes, were used as initial values for the steady-state estimations with the FindRoot function.

The detailed kinetic model and the core model described in this paper are available as supplementary files in SBML (Systems Biology Markup Language) format. In addition, an interactive Web application is provided at www.ibi.vu.nl/sysbio/tpsmodel/, and demonstrates the effects of several parameters on the detailed kinetic model.

Modeling Metabolic Heterogeneity

Model Variations and Random Sampling Descriptions

The kinetic model, as detailed in (*8*), was used to explore the relationship between initial conditions and the probability of obtaining a regular steady state with a model representing the *tps1*Δ state. We took enzyme expression levels and metabolite concentrations as two sources of interindividual metabolic variation in a population. To simulate this heterogeneity, we assumed Gaussian distributions for both enzyme expression levels (represented by V_{max} values) and initial metabolite concentrations. Variance was set such that the probability of a sampled value deviating more than 20% from the reference value is less than 1 in 10^3; this equals a coefficient of variation (that is, a mean-normalized SD) of 6.1% (3.29 SDs = mean ± 20%, for Gaussian distributions). To additionally evaluate the effect of ethanol on the probability of reaching a steady state, we performed samplings at varying ethanol concentrations: 0, 4.3, 10, 21.5, 30, 43, 50, 62.5, 75, 100, 200, and 500 mM.

We randomly drew more than 10^6 unique V_{max} and initial metabolite concentration sets, at each ethanol concentration, and used these as input for the kinetic model. We performed a numerical time simulation for 250 min and evaluated the system to check whether a regular or an imbalanced state was obtained. An imbalanced state was defined when the final FBP concentration was higher than the concentration at 90% of the evaluation time (indicating long-term accumulation). In addition, to score a viable state, free phosphate concentra-

tion >1 mM was used to avoid incorrectly identifying zero flux states as vital steady states, a scenario that would arise when no free phosphate is available to drive FBP accumulation. On the basis of the evaluation outcome, each randomly drawn data set was categorized and saved.

Random sampling, time simulations, and steady-state evaluations were performed, as above, using Mathematica 9.0 (Wolfram Research).

Discriminant Analysis

Using the output from the random sampling evaluations, 5000 samples were drawn (randomly) from the saved data sets, for both imbalanced and regular steady-state solutions, at each ethanol concentration, yielding a data set with 28 variables (14 initial metabolite and 14 V_{max} values) and 24 independent classes (two groups: imbalanced versus steady state, at 12 different ethanol concentrations, see above). The discriminant analysis was performed with the lda function of the MASS package in the R (version 2.14.2) statistical environment (*42*).

References and Notes

1. J. Stelling, U. Sauer, Z. Szallasi, F. J. Doyle III, J. Doyle, Robustness of cellular functions. *Cell* **118**, 675–685 (2004). doi: 10.1016/j.cell.2004.09.008; pmid: 15369668
2. R. J. DeBerardinis, C. B. Thompson, Cellular metabolism and disease: What do metabolic outliers teach us? *Cell* **148**, 1132–1144 (2012). doi: 10.1016/j.cell.2012.02.032; pmid: 22424225
3. A. Flamholz, E. Noor, A. Bar-Even, W. Liebermeister, R. Milo, Glycolytic strategy as a tradeoff between energy yield and protein cost. *Proc. Natl. Acad. Sci. U.S.A.* **110**, 10039–10044 (2013). doi: 10.1073/pnas.1215283110; pmid: 23630264
4. B. Teusink, M. C. Walsh, K. van Dam, H. V. Westerhoff, The danger of metabolic pathways with turbo design. *Trends Biochem. Sci.* **23**, 162–169 (1998). doi: 10.1016/S0968-0004(98)01205-5; pmid: 9612078
5. P. B. Iynedjian, Glycolysis, turbo design and the endocrine pancreatic β cell. *Trends Biochem. Sci.* **23**, 467–468 (1998). doi: 10.1016/S0968-0004(98)01317-6; pmid: 9868365
6. L. Van Aelst *et al.*, Molecular cloning of a gene involved in glucose sensing in the yeast *Saccharomyces cerevisiae*. *Mol. Microbiol.* **8**, 927–943 (1993). doi: 10.1111/j.1365-2958.1993.tb01638.x; pmid: 8355617
7. J. M. Thevelein, S. Hohmann, Trehalose synthase: Guard to the gate of glycolysis in yeast? *Trends Biochem. Sci.* **20**, 3–10 (1995). doi: 10.1016/S0968-0004(00)88938-0; pmid: 7878741
8. See supplementary materials on *Science* Online.
9. S. Hohmann, W. Bell, M. J. Neves, D. Valckx, J. M. Thevelein, Evidence for trehalose-6-phosphate-dependent and -independent mechanisms in the control of sugar influx into yeast glycolysis. *Mol. Microbiol.* **20**, 981–991 (1996). doi: 10.1111/j.1365-2958.1996.tb02539.x; pmid: 8809751
10. B. M. Bonini, P. Van Dijck, J. M. Thevelein, Uncoupling of the glucose growth defect and the deregulation of glycolysis in *Saccharomyces cerevisiae tps1* mutants expressing trehalose-6-phosphate-insensitive hexokinase from *Schizosaccharomyces pombe*. *Biochim. Biophys. Acta* **1606**, 83–93 (2003). doi: 10.1016/S0005-2728(03)00086-0; pmid: 14507429
11. K. Luyten *et al.*, Fps1, a yeast member of the MIP family of channel proteins, is a facilitator for glycerol uptake and efflux and is inactive under osmotic stress. *EMBO J.* **14**, 1360–1371 (1995). pmid: 7729414
12. J. François, J. L. Parrou, Reserve carbohydrates metabolism in the yeast *Saccharomyces cerevisiae*. *FEMS Microbiol. Rev.* **25**, 125–145 (2001). doi: 10.1111/j.1574-6976.2001.tb00574.x; pmid: 11152943
13. B. Teusink *et al.*, Can yeast glycolysis be understood in terms of in vitro kinetics of the constituent enzymes? Testing biochemistry. *Eur. J. Biochem.* **267**, 5313–5329 (2000). doi: 10.1046/j.1432-1327.2000.01527.x; pmid: 10951190
14. S. Hohmann *et al.*, The growth and signalling defects of the *ggs1* (*fdp1/byp1*) deletion mutant on glucose are suppressed by a deletion of the gene encoding hexokinase PII. *Curr. Genet.* **23**, 281–289 (1993). doi: 10.1007/BF00310888; pmid: 8467527
15. J. W. Veening, L. W. Hamoen, O. P. Kuipers, Phosphatases modulate the bistable sporulation gene expression pattern in *Bacillus subtilis*. *Mol. Microbiol.* **56**, 1481–1494 (2005). doi: 10.1111/j.1365-2958.2005.04659.x; pmid: 15916600
16. L. Wang *et al.*, Bistable switches control memory and plasticity in cellular differentiation. *Proc. Natl. Acad. Sci. U.S.A.* **106**, 6638–6643 (2009). doi: 10.1073/pnas.0806137106; pmid: 19366677
17. M. J. Neves *et al.*, Control of glucose influx into glycolysis and pleiotropic effects studied in different isogenic sets of *Saccharomyces cerevisiae* mutants in trehalose biosynthesis. *Curr. Genet.* **27**, 110–122 (1995). doi: 10.1007/BF00313424; pmid: 7788713
18. J. R. S. Newman *et al.*, Single-cell proteomic analysis of *S. cerevisiae* reveals the architecture of biological noise. *Nature* **441**, 840–846 (2006). doi: 10.1038/nature04785; pmid: 16699522
19. S. M. Fendt, U. Sauer, Transcriptional regulation of respiration in yeast metabolizing differently repressive carbon substrates. *BMC Syst. Biol.* **4**, 12 (2010). doi: 10.1186/1752-0509-4-12; pmid: 20167065
20. A. Raj, A. van Oudenaarden, Nature, nurture, or chance: Stochastic gene expression and its consequences. *Cell* **135**, 216–226 (2008). doi: 10.1016/j.cell.2008.09.050; pmid: 18957198
21. N. Q. Balaban, J. Merrin, R. Chait, L. Kowalik, S. Leibler, Bacterial persistence as a phenotypic switch. *Science* **305**, 1622–1625 (2004). doi: 10.1126/science.1099390; pmid: 15308767
22. S. F. Levy, N. Ziv, M. L. Siegal, Bet hedging in yeast by heterogeneous, age-correlated expression of a stress protectant. *PLOS Biol.* **10**, e1001325 (2012). doi: 10.1371/journal.pbio.1001325; pmid: 22589700
23. C. Gancedo, C. L. Flores, The importance of a functional trehalose biosynthetic pathway for the life of yeasts and fungi. *FEMS Yeast Res.* **4**, 351–359 (2004). doi: 10.1016/S1567-1356(03)00222-8; pmid: 14734015
24. M. A. Blázquez, C. Gancedo, Mode of action of the *qcr9* and *cat3* mutations in restoring the ability of *Saccharomyces cerevisiae tps1* mutants to grow on glucose. *Mol. Gen. Genet.* **249**, 655–664 (1995). doi: 10.1007/BF00418035; pmid: 8544831
25. K. M. Overkamp *et al.*, Metabolic engineering of glycerol production in *Saccharomyces cerevisiae*. *Appl. Environ. Microbiol.* **68**, 2814–2821 (2002). doi: 10.1128/AEM.68.6.2814-2821.2002; pmid: 12039737
26. J. M. A. Geertman, J. P. van Dijken, J. T. Pronk, Engineering NADH metabolism in *Saccharomyces cerevisiae*: Formate as an electron donor for glycerol production by anaerobic, glucose-limited chemostat cultures. *FEMS Yeast Res.* **6**, 1193–1203 (2006). doi: 10.1111/j.1567-1364.2006.00124.x; pmid: 17156016
27. A. Abate, R. C. Hillen, S. A. Wahl, Piecewise affine approximations of fluxes and enzyme kinetics from in vivo ^{13}C labeling experiments. *Int. J. Robust Nonlinear Control* **22**, 1120–1139 (2012). doi: 10.1002/rnc.2798
28. J. Londesborough, O. E. Vuorio, Purification of trehalose synthase from baker's yeast. Its temperature-dependent activation by fructose 6-phosphate and inhibition by phosphate. *Eur. J. Biochem.* **216**, 841–848 (1993). doi: 10.1111/j.1432-1033.1993.tb18206.x; pmid: 8404904
29. B. Teusink, H. V. Westerhoff, F. J. Bruggeman, Comparative systems biology: From bacteria to man. *Wiley Interdiscip. Rev. Syst. Biol. Med.* **2**, 518–532 (2010). doi: 10.1002/wsbm.74; pmid: 20836045
30. W. H. Koppenol, P. L. Bounds, C. V. Dang, Otto Warburg's contributions to current concepts of cancer metabolism. *Nat. Rev. Cancer* **11**, 325–337 (2011). doi: 10.1038/nrc3038; pmid: 21508971
31. H. R. Christofk, M. G. Vander Heiden, N. Wu, J. M. Asara, L. C. Cantley, Pyruvate kinase M2 is a phosphotyrosine-binding protein. *Nature* **452**, 181–186 (2008). doi: 10.1038/nature06667; pmid: 18337815
32. M. G. Vander Heiden *et al.*, Evidence for an alternative glycolytic pathway in rapidly proliferating cells. *Science* **329**, 1492–1499 (2010). doi: 10.1126/science.1188015; pmid: 20847263
33. K. van Eunen *et al.*, Measuring enzyme activities under standardized in vivo-like conditions for systems biology. *FEBS J.* **277**, 749–760 (2010). doi: 10.1111/j.1742-4658.2009.07524.x; pmid: 20067525
34. J. P. van Dijken *et al.*, An interlaboratory comparison of physiological and genetic properties of four *Saccharomyces cerevisiae* strains. *Enzyme Microb. Technol.* **26**, 706–714 (2000). doi: 10.1016/S0141-0229(00)00162-9; pmid: 10862876
35. A. B. Canelas, C. Ras, A. ten Pierick, W. M. van Gulik, J. J. Heijnen, An in vivo data-driven framework for classification and quantification of enzyme kinetics and determination of apparent thermodynamic data. *Metab. Eng.* **13**, 294–306 (2011). doi: 10.1016/j.ymben.2011.02.005; pmid: 21354323
36. M. R. Mashego, W. M. van Gulik, J. L. Vinke, D. Visser, J. J. Heijnen, In vivo kinetics with rapid perturbation experiments in *Saccharomyces cerevisiae* using a second-generation BioScope. *Metab. Eng.* **8**, 370–383 (2006). doi: 10.1016/j.ymben.2006.02.002; pmid: 16618549
37. R. H. Schiestl, R. D. Gietz, High efficiency transformation of intact yeast cells using single stranded nucleic acids as a carrier. *Curr. Genet.* **16**, 339–346 (1989). doi: 10.1007/BF00340712; pmid: 2692852
38. R. Orij, J. Postmus, A. Ter Beek, S. Brul, G. J. Smits, In vivo measurement of cytosolic and mitochondrial pH using a pH-sensitive GFP derivative in *Saccharomyces cerevisiae* reveals a relation between intracellular pH and growth. *Microbiology* **155**, 268–278 (2009). doi: 10.1099/mic.0.022038-0; pmid: 19118367
39. J. R. Ernandes *et al.*, During the initiation of fermentation overexpression of hexokinase PII in yeast transiently causes a similar deregulation of glycolysis as deletion of Tps1. *Yeast* **14**, 255–269 (1998). doi: 10.1002/(SICI)1097-0061(199802)14:3<255::AID-YEA228>3.0.CO;2-N; pmid: 9580251
40. W. Wiechert, M. Möllney, N. Isermann, M. Wurzel, A. A. de Graaf, Bidirectional reaction steps in metabolic networks: III. Explicit solution and analysis of isotopomer labeling systems. *Biotechnol. Bioeng.* **66**, 69–85 (1999). doi: 10.1002/(SICI)1097-0290(1999)66:2<69::AID-BIT1>3.0.CO;2-6; pmid: 10567066
41. C. A. Schneider, W. S. Rasband, K. W. Eliceiri, NIH Image to ImageJ: 25 years of image analysis. *Nat. Methods* **9**, 671–675 (2012). doi: 10.1038/nmeth.2089; pmid: 22930834
42. R. Ihaka, R. Gentleman, R: A language for data analysis and graphics. *J. Comput. Graph. Stat.* **5**, 299–314 (1996). doi: 10.2307/1390807

Acknowledgments: We thank G. Smits for pHluorin plasmids; J. Thevelein for W303-1A strains and HXK2 overexpression plasmids; M. Walsh for fruitful discussions; D. Molenaar and H. Hoefsloot for valuable assistance with statistical methods; J. Pronk for experimental suggestions; K. Hellingwerf, R. Leurs, and I. Stulemeijer for critical reading of the manuscript; and L. da Cruz, Z. Zhao, and A. Deshmukh for assistance with tracer experiments. **Funding:** This work was supported by funding from AIMMS, FP7 UNICELLSYS, and Kluyver Centre for Genomics of Industrial Fermentation and NCSB, funded by the Netherlands Genomics Initiatives.

Supplementary Materials

www.sciencemag.org/content/343/6174/1245114/suppl/DC1
Supplementary Text
Figs. S1 to S18
Tables S1 to S8
References (*43*–*57*)

23 August 2013; accepted 7 January 2014
Published online 16 January 2014;
10.1126/science.1245114